Supporting Information

Sato et al. 10.1073/pnas.0811324106

SI Text

SI Results

Protein Isolation. The $A_{280}/A_{\sim 600}$ ratios for fully oxidised WT AZ, and the majority of the other loop variants described in this work (except AZ1A1A, AZ2G2G and AZ2V2V, for the latter because of the presence of 25% zinc) are generally <2. The final yields were ≈2, 20, 0.7, 1.5, 10 and 4 mg/L of cell culture for AZ2G2G, AZ2A2A, AZ2V2V, AZ3A3A, AZ4A3A and AZ4A4A respectively. AZ1A1A did not express well, could not be purified (because of the low amounts produced and multiple forms) and did not bind copper. The mass spectrum of the as-isolated sample did not give a peak ≈13,412 Da (theoretical mass of AZ1A1A with disulfide). However, reduction before mass analysis with Tris(2-carboxyethyl)phosphine hydrochloride resulted in a peak at 13,421 Da. This variant therefore forms disulfide-linked species probably as a consequence of incorrect folding and inherent instability caused by the introduction of a loop that is too short for the scaffold. The A_{280}/A_{614} ratio for pure AZ2G2G is ≈4 and could not be lowered further by oxidation or by the addition of copper (the protein did contain 17% zinc, but this alone cannot explain this high ratio). Pure AZ2G2G gradually lost blue color with time when stored at 4 °C due both to reduction and copper loss. When left for longer periods, the ratio could not be restored by the addition of copper or oxidation. This sample was analyzed on a Superdex 75 column and gave elution volumes corresponding to masses for trimer, dimer and monomer. Furthermore, the very sharp characteristic Trp peak of AZ at 292 nm, which arises from the unique environment of Trp-48 (1), broadened with time in AZ2G2G indicative of protein unfolding. The instability of AZ2G2G prevented a detailed characterization. AZ3A3A eluted from the Superdex 75 column in monomeric and also higher order forms (mainly dimer). These species had almost identical UV/Vis and EPR spectra and therefore the dimeric form still possesses a T1 copper site. MALDI-TOF-MS analysis of the dimer revealed a mass of 13690.5 (theoretical mass of monomeric AZ3A3A = 13695.5) with very little dimer present. Hence the dimeric form of this variant is noncovalently linked (i.e., not involving a disulfide bridge) and would appear to be a precursor to the arrangement seen in the crystallographic studies. Dimeric forms of AZ4A3A and AZ4A4A have also been observed but at much lower levels than in the case of AZ3A3A.

EPR Spectra. EPR simulations, obtained using SIMFONIA (Bruker), which give the parameters listed in Table S1 are shown in Fig. S1. Certain loop variants exhibited >1 T1 copper signal in their EPR spectra. This is particularly obvious for AZ2G2G with the relative amounts of the 2 forms dependent on the amount of glycerol present (see Fig. S2*A*). The major difference is the extra hyperfine line in the g_z region at low field in the absence of glycerol. If this line is included in the simulation in place of the line at highest field then slightly different parameters are obtained ($g_x = 2.040$, $g_y = 2.051$, $g_z = 2.241$, $A_x = 1.0$, $A_y = 1.0$, $A_z = 6.4$), which are more WT-like, and therefore the structural changes are not large. The EPR spectrum of AZ2G2G does not change significantly at glycerol concentrations >40%, and therefore the spectrum shown in Fig. 1*B* (whose parameters are listed in Table S1) is that acquired in 25 mM Hepes pH 7.6 plus 40% glycerol.

In the case of AZ2A2A altering glycerol concentration has a more subtle effect, influencing the intensity of the 4 hyperfine lines in the g_z region of the EPR spectrum (see Fig. S2*B*). The intensity of these lines seems to become more unequal at higher glycerol concentrations and therefore the EPR spectrum of AZ2A2A shown in Fig. 1*B*, and whose parameters are included in Table S1, is that acquired in 50 mM Hepes pH 7.6 without glycerol. The structural changes at the copper site of AZ2A2A indicated by the EPR studies are considerably less than for AZ2G2G.

In the case of AZ3A3A a second set of hyperfine signals in the g_z region from a T1 copper site is apparent in the EPR spectrum in the absence of glycerol (see Fig. S2*C*), that decreases in intensity when glycerol is added. This is similar to what is observed in AZ2G2G but is much less significant, again indicating less flexibility at the active site in AZ3A3A. For AZ2V2V, AZ4A3A and AZ4A4A there was no evidence of a second signal in the EPR spectrum in the absence of glycerol.

NMR Spectra of Cu(II) Proteins. The directly observed hyperfine shifted resonances in the ^{1}H NMR spectra of Cu(II) AZ2A2A and AZ4A4A are all found at similar chemical shifts values as in the WT protein. In the case of AZ2A2A the shifted resonances are considerably sharper than in AZ4A4A and AZ. There was no sign of any additional shifted resonances, as seen in other loop variants of AZ (2, 3) and assigned to $C^{\gamma}H$ protons of the axial Met ligand, in the spectra of AZ2A2A and AZ4A4A.

Reduction Potentials. AZ2A2A yields good quasi-reversible responses on a modified gold electrode over a wide pH range, with anodic and cathodic peaks of equal intensity and separations of typically ≈60 mV at a scan rate of ≈20 mV/s. The E_m value at pH 7.5 is 410 mV. For AZ2G2G a good quasi-reversible response, with anodic and cathodic peaks of equal intensity and a separation of ≈60 mV at a scan rate of ≈20 mV/s is obtained at pH 7.4. The E_m value for AZ2G2G under these conditions is 336 mV. The electrochemical response of AZ2V2V is poor at pH 7.5 but is considerably better at pH 6.5 (separation ≈100 mV at a scan rate of 20 mV/s with equally intense cathodic and anodic peaks) giving an E_m of 426 mV. The electrochemical response of AZ4A3A is less than ideal at pH 7.5 but a reasonably precise E_m of 323 mV can be measured. An improved response (separation of ≈80 mV at a scan rate of 20 mV/s and equally intense anodic and cathodic peaks) was obtained at pH 6 giving an E_m of 369 mV. AZ3A3A and AZ4A4A give generally very poor electrochemical responses under the variety of conditions tested. For AZ3A3A the best response (cathodic and anodic peaks of approximately equal intensity with a separation of ≈80 mV) is obtained on a 3,3′-dithiodipropionic acid modified gold electrode giving an E_m of 332 mV at pH 7.5. This is in good agreement with a value of 344 mV obtained from a redox titration at pH 7.0. In the case of AZ4A4A less than ideal CVs give an E_m of 397 mV at pH 6.5, which is in good agreement with a value of 395 mV from a redox titration at pH 7.0.

Electron Self-Exchange Reactivity of Loop Variants. The electron self-exchange (ESE) rate constants (k_{ESE} values) for AZ2A2A and AZ4A4A have been determined at 40 °C, using ^{1}H NMR spectroscopy. For AZ2A2A the influence of oxidised protein concentration on the T_2^{-1} values of active site resonances arising from the Cu(I) protein in WEFT spectra (4) have been analyzed (see Fig. S3), yielding k_{ESE} values ranging from 3.9×10^4 $M^{-1}{\cdot}s^{-1}$ to 5.6×10^4 $M^{-1}{\cdot}s^{-1}$ and an average of 5.0×10^4 $M^{-1}{\cdot}s^{-1}$. ESE was slower in AZ4A4A, which prevented the use of the WEFT

approach to determine k_{ESE}, because very few resonances were selected in spectra of the reduced protein containing small (2–20%) proportions of the Cu(II) form. An approximate k_{ESE} value was determined from examining broadening of resonances, which exhibit different chemical shift values in the 1D spectra of the Cu(I) and Cu(II) forms in 1:1 mixtures. Analysis of suitable resonances give k_{ESE} values in the range of $1.1 \times 10^4\ M^{-1}{\cdot}s^{-1}$ to $2.5 \times 10^4\ M^{-1}{\cdot}s^{-1}$ and an average of $1.7 \times 10^4\ M^{-1}{\cdot}s^{-1}$. This k_{ESE} value is consistent with the absence of any sign of coalescence for these resonances in the 1:1 mixtures.

SI Materials and Methods

Cell Growth and Initial Protein Isolation. *Escherichia coli* TG1 harbouring pTrcAZ1A1A, pTrcAZ2A2A, pTrcAZ2G2G and pTrcAZ4A4A and JM101 harbouring pTrcAZ2V2V, pTrcAZ3A3A and pTrcAZ4A3A were all grown as described in the presence of 0.5 mM $CuSO_4$ (2). After induction TG1 cells were grown for a further 5 h for pTrcAZ2G2G, 6.5 h for pTrcAZ4A4A and overnight for pTrcAZ1A1A and pTrcAZ2A2A before harvesting. After induction JM101 cultures were grown overnight for pTrcAZ2V2V, 5.5 h for pTrcAZ3A3A and 5 h for pTrcAZ4A3A. The periplasmic proteins were obtained as described in ref. 2.

Isolation and Purification. All proteins were isolated and purified using modifications of the procedure described for AZAMI (2). Fully oxidized AZ2G2G was purified on a Hitrap Q (GE Healthcare), rather than the final DEAE-Sepharose, column. AZ2A2A was loaded onto a Hitrap Q column in place of the second DEAE-Sepharose column. The bound proteins were eluted with 1 mM Tris pH 9.0, using a NaCl gradient of 1–100 mM. A colourless impurity [probably Zn(II) AZ2A2A] was removed on a Resource Q column (GE Healthcare). For this step AZ2A2A in 1 mM Tris pH 9.0 was reduced using ascorbate and loaded onto the column with $<10\ \mu M$ ascorbate present. The bound proteins were eluted with 1 mM Tris pH 9.0, using a NaCl gradient of 1–100 mM, which allowed separation of Zn(II) and Cu(I) forms of the protein. AZ1A1A, AZ2V2V, AZ3A3A and AZ4A4A were isolated and purified by a similar procedure that involved batch extraction, using DEAE-Sepharose, eluted with a 0 to 300 mM NaCl gradient in 1 mM Tris pH 9, a Hitrap Q column eluted with a 0 to 300 mM NaCl gradient in 1 mM Tris pH 9 followed by a Superdex 75 gel filtration column (GE Healthcare) in 20 mM Tris plus 200 mM NaCl pH 8. AZ4A3A was eluted from the DEAE-Sepharose column with 1 mM Tris plus 300 mM NaCl pH 8 and further purified on a HiTrap Q column at pH 8 followed by a Superdex 75 column. The expression level of AZ1A1A was very low and there was no sign of any protein binding a type 1 copper ion (blue color) even after the addition of an excess of Cu(II) and oxidation with a solution of $K_3[Fe(CN)_6]$. Protein eluted over a range of volumes from a Superdex 75 column corresponding to molecular weights in the dimer-tetramer range (no AZ1A1A was found at elution volumes corresponding to the monomeric protein).

Measurement of Reduction Potentials. Electrochemical measurements were typically performed at scan rates of ≈20 mV/s. All E_m values were referenced to the NHE, and voltammograms were calibrated using the $[Co(phen)_3]^{3+/2+}$ couple (370 mV vs. NHE). The gold working electrode was modified using a saturated solution of 4,4-dithiodipyridine (Aldrithiol-4) for AZ2A2A, AZ2V2V and AZ4A3A, and a saturated solution of 3,3′-dithiodipropionic acid for AZ2G2G, AZ2V2V, AZ3A3A and AZ4A4A. In some cases a pyrolytic graphite electrode was used as the working electrode and was prepared and modified with either poly-L-lysine or a mixture of poly-L-lysine and morpholine (8). Cyclic voltammograms (CVs) were measured in 20 mM Tris pH 7.4–7.6 ($I = 0.10$ M, NaCl) for AZ2G2G, AZ2A2A, AZ3A3A and AZ4A3A, and in 20 mM Mes pH 6.5 ($I = 0.10$ M, NaCl) for AZ2V2V and AZ4A4A in 20 mM Mes pH 6.0 ($I = 0.10$ M, NaCl) for AZ4A3A. For the redox titrations with $[Fe(CN)_6]^{3-}$ all buffers were purged with nitrogen and the titrations were performed by adding small aliquots of a 2.5 or 25.5 mM $[Fe(CN)_6]^{3-}$ solution in the same buffer. Additions were made until a final concentration of 1.5 to 2.7 mM $[Fe(CN)_6]^{3-}$.

Crystallization. Cu(II) AZ2A2A was crystallised by the hanging drop method of vapor diffusion at 20 °C, using 1.5 μL of protein (15 mg/mL in 5 mM Tris pH 7.5) mixed with 1.5 μL of precipitant solution (0.1 M potassium thiocyanate, 30% PEG 2000, pH 7.0, well volume 500 μL). Before being frozen in a cold nitrogen stream the crystals were immersed in a cryobuffer comprised of 10% glycerol, 0.1 M potassium thiocyanate, 32% PEG 2000 at pH 6.3. Crystals of Cu(II) AZ2A2A were reduced by transferring them into 20 μL of the reservoir buffer containing 10 mM ascorbate (pH 7.0). Reduction was considered to be complete when the crystal was colourless (typically ≈1 h). The reduced crystals were transferred to cryobuffer containing 10 mM ascorbate (pH 7.0) before being frozen. Cu(II) AZ3A3A was crystallised (at 20 °C) by the sitting drop method of vapor diffusion in 96-well plates set up with a crystallization robot and using 100 nL of protein mixed with either 100 or 200 nL of precipitant solution (150 mM potassium bromide, 30% PEG MME 2000, well volume 100 μL). Before being frozen in a cold nitrogen stream the crystals were immersed in *N*-paratone oil. Cu(II) AZ4A3A was crystallised by the hanging drop vapor diffusion method at 20 °C, using 1.5 μL of protein (15 mg/mL in 5 mM Tris pH 7.5) mixed with 1.5 μL of precipitant solution (100 mM Hepes pH 8.0 plus 34% PEG 4000, well volume 500 μL). Crystals were frozen directly in liquid nitrogen before data collection. Cu(II) AZ4A4A (14 mg/mL in 5 mM Tris pH 7.5) was crystallised by sitting drop vapor diffusion in 96-well plates, which had been set up by a crystallization robot (1:1 protein to precipitant; 10 mM tri-sodium citrate, 33% PEG 6000, pH ≈ 7.6, well volume 100 μL). Before being frozen in a nitrogen stream, Cu(II) AZ4A4A crystals were immersed in a cryobuffer consisting of 5% glycerol, 10 mM tri-sodium citrate, 33% PEG 6000. AZ4A4A crystals were also obtained by hanging drop vapor diffusion at 20 °C, using 2.0 μL of protein (as above) mixed with 2.0 μL of precipitant solution (as above; well volume 300 μL). These crystals were reduced by transferring them into 15 μL of the reservoir buffer containing 10 mM ascorbate (pH 7.0). Reduction was considered to be complete when the crystal was colourless (typically ≈1 h). The reduced crystals were transferred to cryobuffer containing 10 mM ascorbate (pH 7.5) before being frozen.

Protein crystals were maintained at cryogenic temperatures during data collection. Diffraction data were collected using the following experimental set-ups (datasets and regimens are given in Table S5):

1. ESRF: ESRF, beamline ID14–4 equipped with an ADSC Q315 3 × 3 CCD detector.
2. DLS: Diamond Light Source, beamline I03 equipped with an ADSC Q315 3 × 3 CCD detector.
3. Norwich: X-rays from a Rigaku RU-H3RHB generator with Osmic optics and a MAR-345 image plate detector.
4. Newcastle: X-rays from a Rigaku Micromax-007 generator with Osmic optics and a Rigaku Raxis IV^{++} image plate detector.

Throughout this article, the description of a Cu(II) structure means that the protein was oxidised (crystals blue in color) immediately before data collection (with the exception of the AZ3A3A crystal, which was colourless). Rapid photo-reduction of metal sites in protein crystals can occur on exposure to X-rays (especially when using high intensity synchrotron radiation sources) (9, 10). It is probable that the proteins crystallised as Cu(II) in this study underwent some degree of photo-reduction during data collection. All data were processed with MOSFLM/iMOSFLM (11) and scaled with SCALA (12). Data collection and processing statistics are given in Table S5. Structures were solved by molecular replacement/direct refinement. The Cu(II) AZ2A2A structure was solved using MolRep [as implemented in CCP4 (13)] and the structure of AZAMI-F [PDB entry 2FT6 (3)], with the C-terminal ligand-containing loop removed, as the search model. The final Cu(II) AZ2A2A structure was used as a starting model for refinement of the Cu(I) AZ2A2A structure. The AZ3A3A structure was solved using Phaser [as implemented in CCP4 (14)] with the final Cu(II) AZ2A2A structure, with the C-terminal ligand-containing loop removed, as the search model. The AZ4A3A structure was solved using Phaser and the structure of AZAMI-F [PDB entry 2FT6 (3)], with the C-terminal ligand-containing loop removed, as the search model. The Cu(II) AZ4A4A structure was solved using the same regimen as AZ3A3A, and the final Cu(II) AZ4A4A structure was used as a starting model for refinement of the Cu(I) AZ4A4A structure. Iterative model building [using Coot (15)] and refinement [Refmac5, as implemented in CCP4] cycles were used to complete all structures (16, 17). In the final stages of refining the Cu(II) and Cu(I) AZ2A2A structures, anisotropic B-factors were refined while monitoring both the R_{factor} and R_{free}. Final refinement statistics are given in Table S5.

1. Sweeney JA, Harmon PA, Asher SA, Hutnik CM, Szabo AG (1991) UV resonance Raman examination of the azurin tryptophan environment and energy relaxation pathways. *J Am Chem Soc* 113:7531–7537.
2. Yanagisawa S, Dennison C (2004) Loop-contraction mutagenesis of type 1 copper sites. *J Am Chem Soc* 126:15711–15719.

3. Li C, et al. (2006) Basic requirements for a metal-binding site in a protein: the influence of loop shortening on the cupredoxin azurin. *Proc Natl Acad Sci USA* 103:7258–7263.
4. Sato K, Kohzuma T, Dennison C (2003) Active-site structure and electron-transfer reactivity of plastocyanins. *J Am Chem Soc* 125:2101–2112.
5. Groeneveld CM, Canters GW (1985) The pH dependence of the electron self-exchange rate of azurin from *Pseudomonas aeruginosa* as studied by ^{1}H-NMR. *Eur J Biochem* 153:559–564.
6. van de Kamp M, et al. (1993) Effect of lysine ionization on the structure and electrochemical behaviour of the Met44→Lys mutant of the blue-copper protein azurin from *Pseudomonas aeruginosa*. *Eur J Biochem* 218:229–238.
7. Nar H, Messerschmidt A, Huber R, van de Kamp M, Canters GW (1991) Crystal structure analysis of oxidized *Pseudomonas aeruginosa* azurin at pH 5.5 and pH 9.0. *J Mol Biol* 221:765–772.
8. Battistuzzi G, et al. (2002) Thermodynamics of the acid transition in blue copper proteins. *Biochemistry* 41:14293–14298.
9. Ellis MJ, Buffey SG, Hough MA, Hasnain SS (2008) On-line optical and X-ray spectroscopies with crystallography: an integrated approach for determining metalloprotein structures in functionally well defined states. *J Synchrotron Rad* 15:433–439.
10. Strange RW, Feiters MC (2008) Biological X-ray absorption spectroscopy (BioXAS): a valuable tool for the study of trace elements in the life sciences. *Curr Opin Struct Biol* 18:609–616.
11. Leslie AG (2006) The integration of macromolecular diffraction data. *Acta Crystallogr D Biol Crystallogr* 62:48–57.
12. Evans P (2006) Scaling and assessment of data quality. *Acta Crystallogr D Biol Crystallogr* 62:72–82.
13. Vagin A, Teplyakov A (1997) MOLREP: an automated program for molecular replacement. *J Appl Cryst* 30:1022–1025.
14. McCoy AJ (2007) Solving structures of protein complexes by molecular replacement with Phaser. *Acta Crystallogr D Biol Crystallogr* 63:32–41.
15. Emsley P, Cowtan K (2004) Coot: Model-building tools for molecular graphics. *Acta Crystallogr D Biol Crystallogr* 60:2126–2132.
16. Murshudov GN, Vagin AA, Dodson EJ (1997) Refinement of macromolecular structures by the maximum-likelihood method. *Acta Crystallogr D Biol Crystallogr* 53:240–255.
17. Collaborative computational project (1994) *Acta Crystallogr D Biol Crystallogr* 50:760–763.

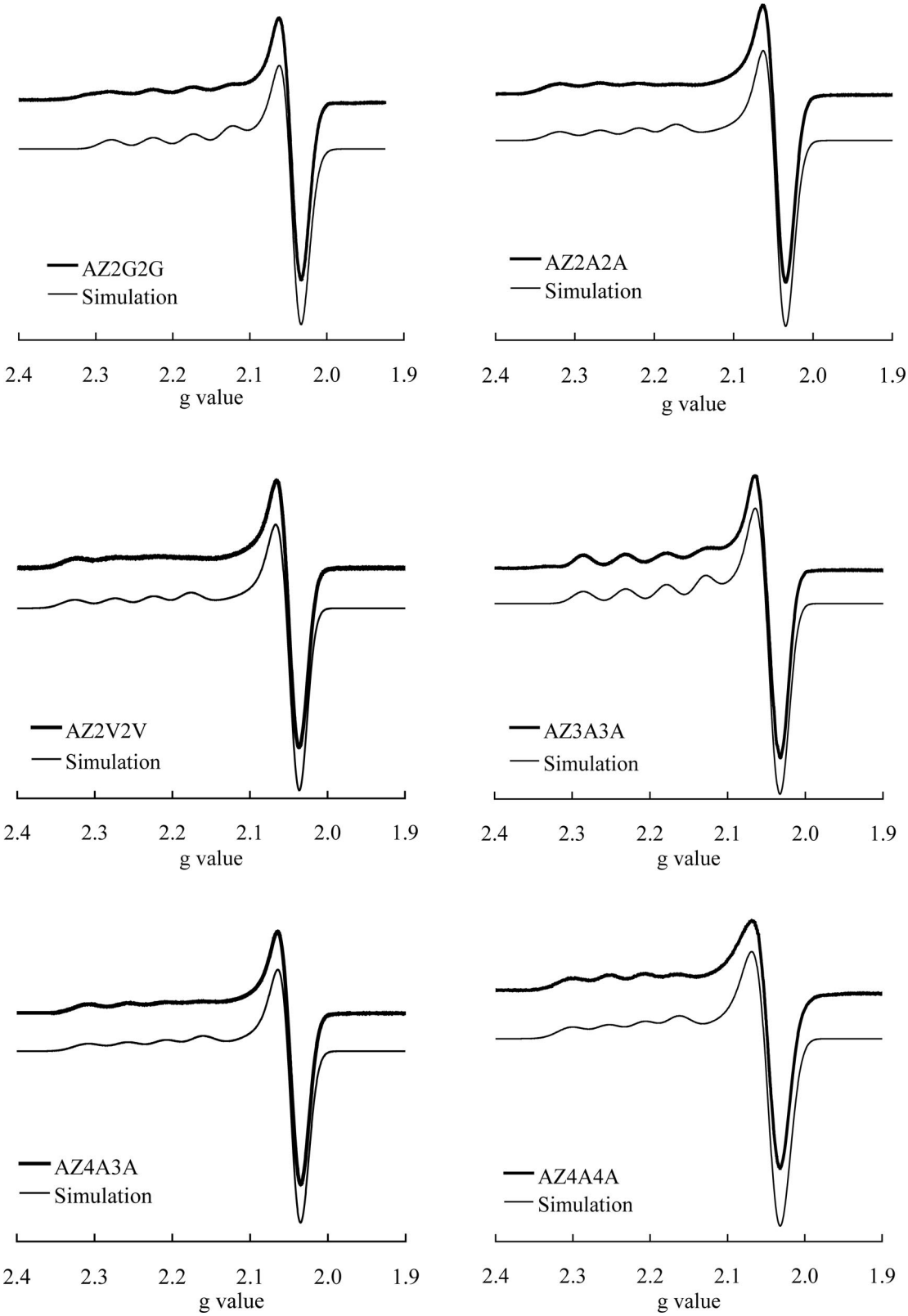

Fig. S1. X-band EPR spectra (−196 °C) in 25 mM Hepes pH 7.6 (40% glycerol) for AZ2G2G and AZ3A3A, and 50 mM Hepes pH 7.6 for all other proteins. Also shown are the simulated spectra obtained using SimFonia (Bruker) and the parameters obtained are shown in Table S1.

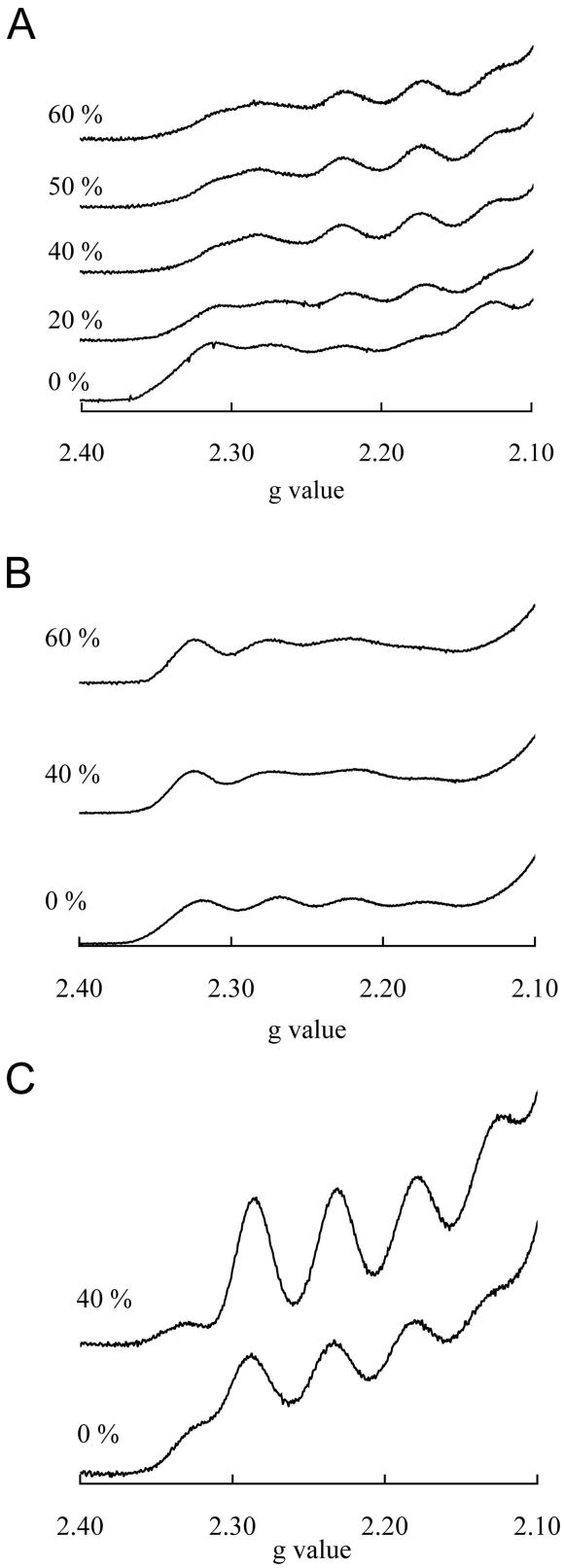

Fig. S2. The influence of glycerol on the g_z region of the EPR spectra (−196 °C) of AZ2G2G (*A*), AZ2A2A (*B*) and AZ3A3A (*C*). Spectra were obtained in 20–50 mM Hepes pH 7.6 plus the percentage of glycerol shown.

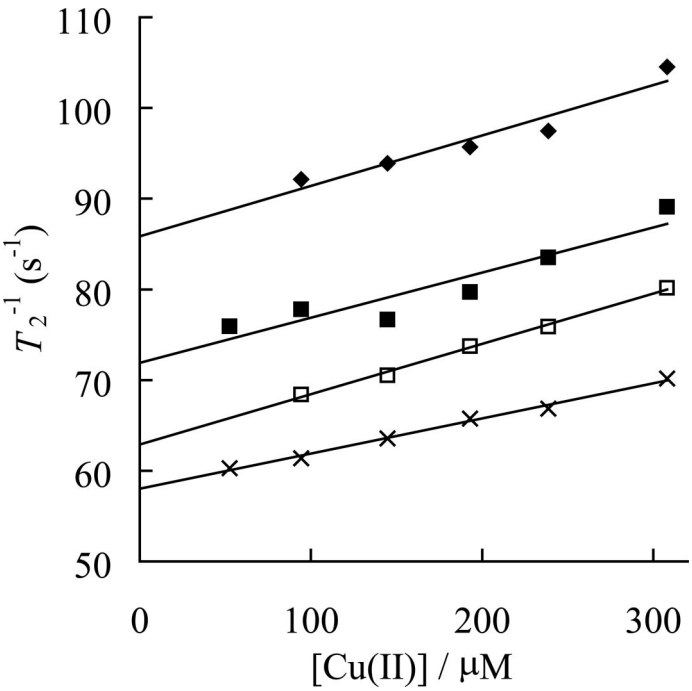

Fig. S3. Plots (40 °C) of T_2^{-1} (s^{-1}) against [Cu(II)] for the signals at 9.34 (filled diamonds), 7.50 (open squares), 6.15 (×, possibly the His-115 $C^{\varepsilon 1}H$ resonance) and 0.07 (filled squares; the Met-118 $C^{\varepsilon}H_3$ resonance) ppm in the WEFT spectrum of Cu(I) AZ2A2A in 10 mM phosphate (99.9% D_2O) pH* 8.0. Self-exchange rate constants (k_{ESE} values) were obtained using the following equation (which is valid for protons belonging to the slow exchange regime); $T_{2,obs}^{-1} = T_{2,red}^{-1} + k_{ESE}[Cu(II)]$, where $T_{2,obs}^{-1}$ is the observed transverse relaxation rate of a resonance, $T_{2,red}^{-1}$ is the observed relaxation rate in the fully reduced protein, and [Cu(II)] is the concentration of oxidised protein.

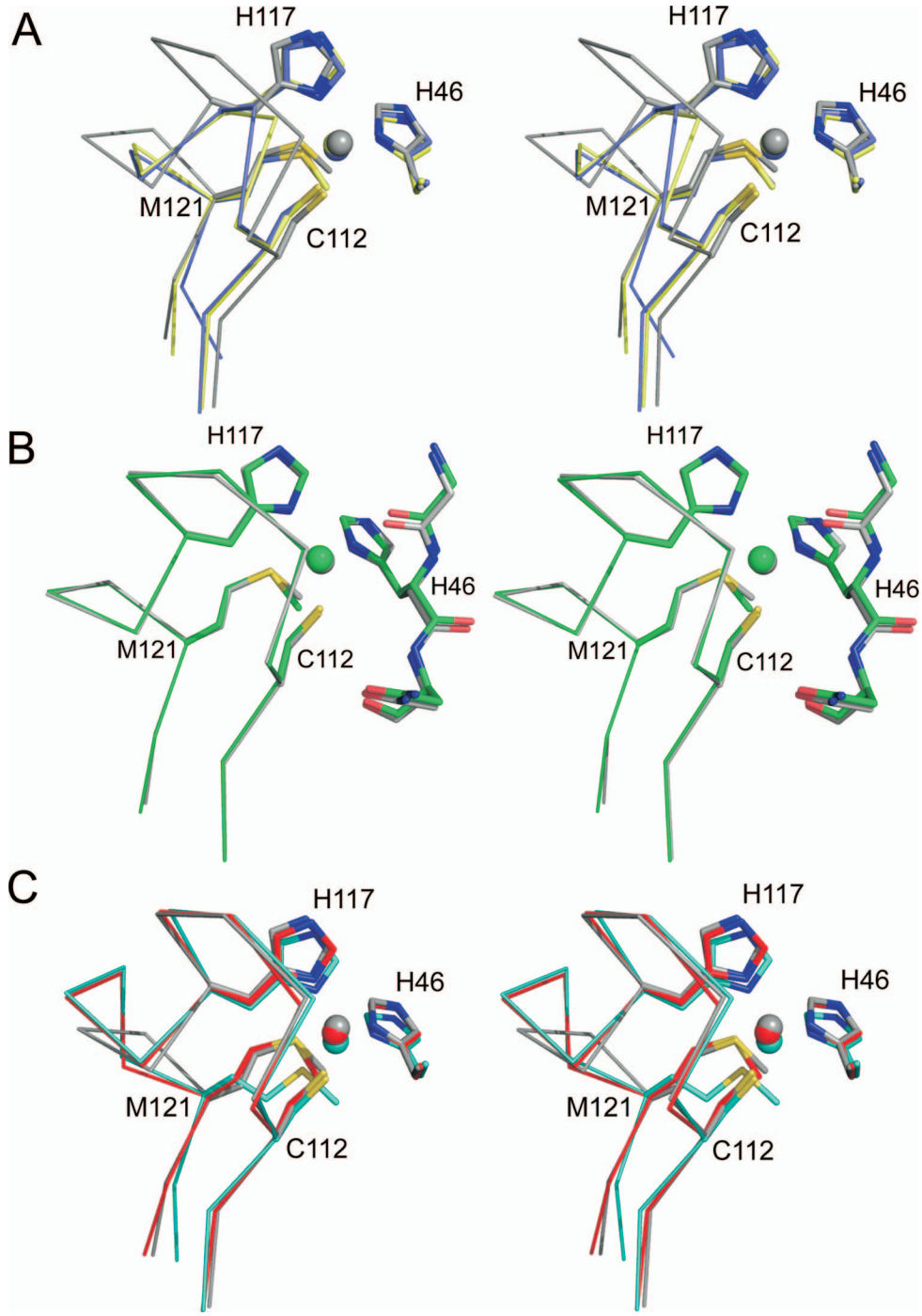

Fig. S4. Stereoviews of the superimposed Cu(II) sites of AZ (4AZU, chain A, gray), AMI (1AAC, yellow) and AZ2A2A (slate) (*A*); AZ (4AZU, chain A, gray) and AZ4A3A (green) (*B*); and AZ (4AZU, chain A, gray), auracyanin B (1QHQ, cyan) and AZ4A4A (red) (*C*). The side chains of the coordinating residues (Gly-45 omitted in *A* and *C*), and those of the amino acids on either side of the N-terminal His ligand (*B* only) are shown as stick models, copper atoms as spheres, and the backbone of the C-terminal ligand-containing loop as C^{α} traces. Ligands are numbered as in AZ.

Table S1. Properties of the loop variants of AZ compared with the WT protein

Parameter	AZ	AZAMI*	AZ2G2G	AZ2V2V	AZ2A2A	AZ3A3A	AZ4A3A	AZ4A4A
Mass								
MALDI-TOF-MS			13,497.2	13,666.4	13,556.7	13696.5	13,770.9	13,844.9
Theoretical†			13,498.3	13,666.6	13,554.4	13696.5	13,767.7	13,838.7
UV/vis‡								
λ_{max1}, nm	460(sh)	470(sh)	460(sh)	478(sh)	460(sh)	460(sh)	460(sh)	460(sh)
λ_{max2}, nm	628	609	614	622	624	614	616	614
$\varepsilon_{\sim 600}$, $mM^{-1}{\cdot}cm^{-1}$	5.1	4.5	5.4	5.3	5.3	5.3	4.9	5.0
$A_{\sim 460}/A_{\sim 600}$	0.07	0.07	0.08	0.07	0.07	0.07	0.05	0.08
EPR§								
g_x	2.035	2.033	2.042	2.046	2.040	2.033	2.042	2.043
g_y	2.054	2.048	2.047	2.048	2.047	2.054	2.049	2.047
g_z	2.261	2.225	2.200	2.249	2.244	2.205	2.233	2.232
A_x, mT	1.4	1.1	0.5	1.0	1.0	0	0	0.8
A_y, mT	1.4	1.0	0.5	0.9	0.6	0	0	0.6
A_z, mT	5.3	6.9	7.2	6.6	6.5	7.2	6.6	6.2
Azide binding¶								
K_d, M		8.4	0.3	6.8	2.4			
E_m value, mV‖	295	261	336	426	410	344	323	395
k_{ESE} ($M^{-1}{\cdot}s^{-1}$)**	2.0×10^6	5.5×10^5			5.0×10^4			1.7×10^4

*Data for AZAMI taken from Yanagisawa and Dennison [(2004) *J Am Chem Soc* 126:15711–15719].

†Theoretical mass considers a disulfide bond present between Cys3 and Cys24.

‡Data for AZ recorded in 10 mM phosphate pH 8.0 while that for AZ2G2G, AZ2V2V, and AZ2A2A was measured in 20 mM Tris pH 8.0, that for AZ3A3A and AZ4A4A in 50 mM Hepes pH 7.6.

§The data for AZ, AZ2G2G and AZ3A3A were recorded in 25 mM Hepes pH 7.6 containing 40% glycerol while those for AZ2V2V, AZ2A2A and AZ4A4A were measured in 50 mM Hepes pH 7.6. All of the EPR parameters were derived from simulations using the program SIMFONIA (Bruker).

¶Measured in 20 mM Tris pH 8.0 at 25 °C.

‖Measured at 22 ± 1°C in 20 mM Tris at pH 7.5 (I = 0.10 M, NaCl) for AZ, AZAMI and AZ4A3A; 20 mM Tris at pH 7.4 (I = 0.10 M, NaCl) for AZ2G2G; 20 mM Mes at pH 6.5 (I = 0.10 M, NaCl) for AZ2V2V; 20 mM Tris at pH 7.6 (I = 0.10 M, NaCl) for AZ2A2A; 50 mM phosphate pH 7.0 (I = 0.11 M) for AZ3A3A and AZ4A4A.

**Electron self-exchange rate constant (k_{ESE}) measured at 40°C in 20 mM phosphate pH* 8.0 for AZ (5). The value for AZAMI was determined in 20 mM phosphate pH* 8.2 at 25°C and the k_{ESE} value for AZ under these conditions is 7×10^5 $M^{-1}s^{-1}$, which is almost the same in 10 mM phosphate (5, 6). The k_{ESE} of AZ2A2A was determined in 10 mM phosphate (pH* 8.0) at 40 °C while that of AZ4A4A was measured in 20 mM phosphate pH* 8.0 at 40 °C.

Table S2. The geometry of the type 1 Cu(II) sites of AZ2A2A, AZ4A3A, AZ4A4A, AZAMI and AZ

	AZ (4AZU)*	AZAMI (2FTA)†	AZ2A2A‡	AZ4A3A§	AZ4A4A¶
Cu(II)—ligand bond distances, Å					
Cu–O(Gly45)	2.97	3.19	3.49	3.23	3.23
Cu–$N^{\delta 1}$(His46)	2.08	1.98	2.00	2.00	2.09
Cu–S^{γ}(Cys112)	2.24	2.14	2.20	2.13	2.13
Cu–$N^{\delta 1}$(His117)	2.01	2.09	2.02	2.03	2.14
Cu–S^{δ}(Met121)	3.15	3.29	3.02	3.26	3.31
Cu–NSN plane‖	0.08	0.14	0.23	0.14	0.15
Angle, deg					
Gly45–Cu–His46	74	79	70	74	76
Gly45–Cu–Cys112	99	97	100	99	98
Gly45–Cu–His117	89	81	79	83	78
Gly45–Cu–Met121	148	151	147	147	146
His46-Cu-Cys112	132	134	133	133	136
His46-Cu-His117	105	102	103	102	101
His46-Cu-Met121	77	76	81	75	75
Cys112-Cu-His117	123	123	120	124	122
Cys112-Cu-Met121	110	112	113	112	117
His117-Cu-Met121	87	92	91	90	85
ϕ**	84	81	84	81	85

*_Pseudomonas aeruginosa_ Cu(II) AZ at pH 5.5 (average of 4 chains) (7).
†Cu(II) AZAMI at pH 7 in which His117 and Met121 are replaced by His115 and Met118 (average of 4 chains) (3).
‡Cu(II) AZ2A2A at pH 7 in which His117 and Met121 are replaced by His115 and Met118.
§Average of the 4 chains in the Cu(II) AZ4A3A structure at pH 8.
¶Average of the the 2 chains in the Cu(II) AZ4A4A structure at pH 7.6 in which Met121 is replaced by Met122.
‖Displacement of the copper ion from the plane containing the coordinating atoms of His46, Cys112 and His117 (numbering as in AZ).
**The angle between the $N_{His}CuN_{His}$ and $S_{Cys}CuS_{Met}$ planes.

Table S3. The geometry of the type 1 Cu(I) sites of AZ2A2A, AZ4A4A and AZ

	AZ (1E5Y)*	AZ2A2A†	AZ4A4A‡
Cu(I)–ligand bond distances, Å			
Cu–O(Gly45)	3.02	3.49	3.36
Cu–$N^{\delta 1}$(His46)	2.14	2.03	2.12
Cu–S^{γ}(Cys112)	2.29	2.21	2.19
Cu–$N^{\delta 1}$(His117)	2.10	2.02	2.10
Cu–S^{δ}(Met121)	3.25	3.04	3.23
Cu–NSN plane§	0.09	0.24	0.16
Angle (deg)			
Gly45–Cu–His46	75	71	75
Gly45–Cu–Cys112	99	98	99
Gly45–Cu–His117	87	79	81
Gly45–Cu–Met121	145	148	144
His46-Cu-Cys112	133	131	138
His46-Cu-His117	105	102	99
His46-Cu-Met121	73	81	75
Cys112-Cu-His117	122	122	123
Cys112-Cu-Met121	114	112	117
His117-Cu-Met121	88	93	84

*_Pseudomonas aeruginosa_ Cu(I) AZ at pH 5.5 (average of 4 chains) (7).
†Cu(I) AZ2A2A at pH 7 in which His117 and Met121 are replaced by His115 and Met118.
‡Average of the 2 chains in Cu(I) AZ4A4A at pH 7.7 in which Met121 is replaced by Met122.
§Displacement of the copper ion from the plane containing the coordinating atoms of His46, Cys112 and His117 (numbering as in AZ).

Table S4. Primers used to make the loop mutations

Primer	Sequence (5′ to 3′)
$C^{112}AH^{114}AM^{116}$ (forward)	catgttcttctgcgcgcacgcgatgaagggcacc
$C^{112}AH^{114}AM^{116}$ (reverse)	ggtgcccttcatcgcgtgcgcgcagaagaacatg
$C^{112}AAH^{115}AAM^{118}$ (forward)	catgttcttctgcgccgcgcacgcggccatgaagggcacc
$C^{112}AAH^{115}AAM^{118}$ (reverse)	ggtgcccttcatggccgcgtgcgcggcgcagaagaacatg
$C^{112}GGH^{115}GGM^{118}$ (forward)	catgttcttctgcggcggccacggcggcatgaagggcacc
$C^{112}GGH^{115}GGM^{118}$ (reverse)	ggtgcccttcatgccgccgtggccgccgcagaagaacatg
$C^{112}VVH^{115}VVM^{118}$ (forward)	catgttcttctgcgttgttcacgttgttatgaagggcacc
$C^{112}VVH^{115}VVM^{118}$ (reverse)	ggtgcccttcataacaacgtgaacaacgcagaagaacatg
$C^{112}AAAH^{116}AAAM^{120}$ (forward)	catgttcttctgcgcggccg cgcacgcggccgcgatgaagggcacc
$C^{112}AAAH^{116}AAAM^{120}$ (reverse)	ggtgcccttcatcgcggccgcgtgcgcggccgcgcagaagaacatg
$C^{112}AAAAH^{117}AAAM^{121}$ (forward)	gttcttctgcgcggcggccgcgcacgcggccgcggcgatgaagggcacc
$C^{112}AAAAH^{117}AAAM^{121}$ (reverse)	ggtgcccttcatcgccgcggccgcgtgcgcggccgccgcgcagaagaac
$C^{112}AAAAH^{117}AAAAM^{122}$ (forward)	gttcttctgcgcggcggccgcgcacgcggccgcggcgatgaagggcacc
$C^{112}AAAAH^{117}AAAAM^{122}$ (reverse)	ggtgcccttcatcgccgcggccgcgtgcgcggccgccgcgcagaagaac

Table S5. Crystallographic data collection, processing and refinement statistics

	Cu(II) AZ2A2A	Cu(I) AZ2A2A	AZ3A3A	Cu(II) AZ4A3A	Cu(II) AZ4A4A	Cu(I) AZ4A4A
Instrumentation	ESRF	ESRF	DLS	Norwich	Newcastle	Newcastle
Wavelength, Å	0.98	0.98	0.97	1.54	1.54	1.54
Space group	$P2_12_12_1$	$P2_12_12_1$	$I222$	$P1$	$P2_1$	$P2_1$
Resolution, Å	58.0–1.05 (1.11–1.05)	46.3–0.98 (1.03–0.98)	44.7–2.30 (2.42–2.30)	49.8–2.00 (2.10–2.00)	23.1–2.00 (2.11–2.00)	23.1–1.80 (1.90–1.80)
Unit cell parameters						
a, Å	39.77	40.14	53.84	36.67	34.82	34.66
b, Å	46.16	46.31	55.82	56.70	86.96	86.99
c, Å	58.03	58.10	74.48	58.24	41.84	42.16
α, °				111.96		
β, °				95.38	113.82	114.67
γ, °				105.12		
No. of unique reflections	50,521 (7,235)	61,635 (7,766)	5,240 (755)	25,606 (3,332)	13,807 (1,851)	17,866 (2,509)
Redundancy	10.5 (8.7)	10.7 (5.3)	11.2 (11.4)	3.9 (3.8)	6.2 (6.3)	4.8 (4.9)
$I/\sigma(I)$	24.5 (9.1)	27.9 (8.6)	21.8 (7.4)	11.9 (5.4)	18.7 (5.0)	18.5 (3.6)
Completeness, %	99.5 (99.0)	97.8 (85.9)	100 (100)	91.7 (81.5)	89.9 (83.2)	85.3 (82.3)
R_{merge}, %	5.6 (23.9)	5.6 (14.2)	10.3 (37.3)	9.2 (26.6)	9.4 (32.8)	7.1 (34.8)
Resolution, Å	33.0–1.05 (1.08–1.05)	33.0–0.98 (1.01–0.98)	44.7–2.30 (2.36–2.30)	49.8–2.00 (2.06–2.00)	21.4–2.00 (2.05–2.00)	21.8–1.80 (1.85–1.80)
R_{factor}, %	12.0 (21.4)	12.0 (14.0)	25.7 (30.7)	18.9 (24.1)	18.4 (19.8)	18.9 (26.3)
R_{free}, %	14.5 (27.2)	13.5 (16.7)	30.8 (35.1)	25.6 (29.5)	25.5 (27.9)	25.0 (44.8)
rmsd bond lengths, Å	0.018	0.018	0.007	0.009	0.009	0.012
rmsd bond angles, °	1.9	1.8	0.97	1.13	1.15	1.33
No. of non-hydrogen atoms	1281	1211	904	4017	2226	2208
Average *B*-factor (protein), Å^2	8.2	8.1	33.1	15.0	14.6	17.0
Average *B*-factor (ligands), Å^2	19.1	18.7	28.0	16.4	22.4	24.0
ESU (maximum likelihood), Å^2	0.014	0.010	0.236	0.153	0.14	0.11
Ramachandran favoured, %	98.4	97.5	99.1	97.0	97.2	97.3
Ramachandran outliers, %	0.0	0.0	0.0	0.0	0.0	0.0

Values in parentheses are for the highest resolution shell.